X-ray-pulse characterization by spectral shearing interferometry using three-wave mixing

S. Yudovich and S. Shwartz*

Department of Physics, Institute for Nanotechnology and Advanced Materials, Bar Ilan University, Ramat Gan 52900, Israel

(Received 17 June 2014; published 3 September 2014)

We describe a method for measuring the field profile of x-ray ultrashort pulses including phase information. The scheme is based on spectrally interfering two replicas of the same pulse, which are spectrally shifted via three-wave mixing with IR or visible beams. Using a single-shot spectrometer the scheme can be used for the inspection of individual ultrashort x-ray pulses with random amplitudes and phases. Examples for characterization of stochastic pulses with a bandwidth of 1 eV are given, including criteria for a successful measurement.

DOI: 10.1103/PhysRevA.90.033805 PACS number(s): 42.65.Re, 41.50.+h, 42.65.Ky

X-ray free-electron lasers (XFELs) producing intense ultrashort pulses have become operative [1,2] and have opened new possibilities for probing and imaging structures and dynamics of matters on a time scale of tens of femtoseconds [3–6]. Indeed, the number of experiments and theoretical studies relying on ultrashort pulses at x-ray wavelengths is growing rapidly. Complete pulse characterization, including both amplitude and phase, could be essential when analyzing the results of those experiments. For example, intense x-ray spikes can modify the electronic configuration in matter via photoabsorption and recombination processes occurring on a femtosecond time scale [7]. Since any pulse emerging from a self-amplified spontaneous emission- (SASE-) based XFEL contains a large number of randomly distributed spikes over a duration of several femtoseconds, the electrons do not return to their original configuration between the spikes. Consequently, the interpretation of the ultrafast electronic response to x-ray pulses requires the knowledge of the temporal structure of the pulses. In addition, the understanding of the temporal structure of the pulses emerging from the XFELs will improve their performances in a manner similar to the contributions of ultrafast diagnostic techniques to lasers in the optical regime. Other fields where the phase variation in the pulse and its temporal coherence are important are related to coherent processes in both electronic and nuclear interactions with x rays [8,9].

Methods for the full characterization of ultrashort pulses have been shown to be very successful in a broad spectral range from infrared wavelengths to ultraviolet wavelengths. Methods, such as frequency-resolved optical gating, spectral phase interferometry for direct electric-field reconstruction (SPIDER) and their variations, have been highly successful in complete characterization of ultrashort pulses [10,11]. Many of these methods rely on the rapid response of a nonlinear process of electrons in materials as an essential component in their scheme.

Unfortunately, nonlinear processes, such as second-harmonic generation [12] and two-photon absorption [13], are very weak in the x-ray regime. In addition, the random and spiky nature of the XFEL pulses requires single-shot characterization of the temporal structure. Thus in the absence of detectors with subfemtosecond response times, the temporal characterization of x-ray pulses is extremely difficult.

Several methods have been proposed or demonstrated for the characterization of x-ray pulses. Some approaches involve the same electron beam, used for the generation of the XFEL radiation, in which its energy loss and spread are temporally resolved [14] or the electron beam cross correlated with the x-ray field [15]. Another approach is a terahertz streaking measurement technique in which single-cycle terahertz pulses are used in order to spectrally broaden the kinetic-energy distribution of photoelectrons ejected by the x-ray pulse, having its temporal profile [16]. However, those methods do not provide phase information, and their temporal resolution is limited to above the few hundred attosecond pulse duration predicted for SASE XFEL spikes.

Before we proceed, we note a scheme proposed for the measurement of attosecond soft x-ray pulses. That scheme is based on the coherent generation of photoelectrons which contain the phase information of their generating x-ray pulse. This effect has led to the proposal of implementing a spectral shearing interferometry scheme to the wave packets of those photoelectrons [17] where the spectral shift is achieved by a strong optical laser.

In this paper, we describe a method for the measurement of the full temporal structure of x-ray pulses with the global phase being the only ambiguity. Like other schemes based on spectral shearing interferometry, the scheme we propose is inherently applicable for single-shot measurements, and the algorithm for the reconstruction of the temporal structure is straightforward. In essence, in this scheme the measured x-ray pulse is mixed with two synchronized optical pulses at different frequencies in the same nonlinear medium to generate two spectrally shifted pulses. These two spectrally shifted replicas of the incident pulse form a spectral interference pattern, which is resolved by a single-shot spectrometer. The generation of the two replicas can be performed by using the effect of x-ray and optical wave mixing [18]. This recently observed effect is about four orders of magnitude stronger than other wave-mixing effects when all pertinent wavelengths are in the x-ray regime. Of importance, since the efficiency of the x-ray and optical mixing depends on the intensity of the optical lasers and since high power optical lasers are available today, the effect can be observed with all pertinent beams unfocused and with optical pulse durations of several picoseconds. Hence our

*Sharon.shwartz@biu.ac.il

scheme is independent of the jitter of the x-ray pulses, and the spatiotemporal phase distortion during the nonlinear process due to focusing is minimized.

The temporal pulse structure $E(t)$ can be fully represented by its spectrum via a Fourier transform, namely, $\tilde{E}(\omega) = A(\omega)e^{i\varphi(\omega)}$. Here $A(\omega)$ is the spectral amplitude, and $\varphi(\omega)$ is the spectral phase. Consequently, the full characterization of ultrashort pulses can be obtained by the measurements of both the spectral amplitude and the spectral phase of the electric field. The measurement of the spectral amplitude is relatively easy and usually is performed by using a spectrometer with a slow detector, which is an advantage when characterizing ultrashort pulses having a temporal duration shorter than the possible electronic response time. The measurement of the phase is more challenging mainly because interferometers with slow detectors measure only the power spectrum of the pulse. In order to retrieve the spectral phase, spectral interference between two spectrally shifted replicas of the tested pulse is being used in devices based on SPIDER techniques [10,19]. Generally, the power spectrum of the superposition of two spectrally shifted replicas $\tilde{E}(\omega - \Omega_1)$ and $\tilde{E}(\omega - \Omega_2)$ of the test pulse has the form of

$$\begin{aligned} I(\omega) &\sim |e^{i\phi_1}\tilde{E}(\omega-\Omega_1) + e^{i(\phi_2+\omega\tau)}\tilde{E}(\omega-\Omega_2)|^2 \\ &= [A(\omega-\Omega_1)]^2 + [A(\omega-\Omega_2)]^2 \\ &\quad + 2A(\omega-\Omega_1)A(\omega-\Omega_2)\cos[\varphi(\omega-\Omega_1) \\ &\quad - \varphi(\omega-\Omega_2) + \phi_1 - \phi_2 - \omega\tau], \end{aligned} \tag{1}$$

where Ω_1 and Ω_2 are the spectral shift of each of the replicas, ϕ_1 and ϕ_2 are the global phase of each replica, and τ is a possible temporal delay between them. Extracting $\varphi(\omega-\Omega_1) - \varphi(\omega-\Omega_2)$, one obtains the phase difference between spectral components $\Delta\Omega = \Omega_2 - \Omega_1$ apart. In essence, spectral shearing interferometry converts spectral phase information to spectral amplitude information, which is easier to measure. This straightforward noniterative reconstruction process gives the pulse spectrum at sequential points $\tilde{E}(\omega_n)$, where $\omega_n = \omega_0 + \Delta\Omega\, n$ with ω_0 being a certain starting point. For pulses with compact support over a duration of T, the Nyquist-Shannon sampling theorem states that, if the sampling in the spectral domain is carried out with an interval of $\Delta\Omega \leqslant \frac{2\pi}{T}$, the original pulse $E(t)$ may be fully reconstructed. Note that since only phase differences between sequential points are measured, this method does not account for the global phase or, equivalently, the pulse arrival time.

Our scheme is based on the spectral interference between two frequency-shifted signals. One possible way to generate these signals in the x-ray regime is to use the effect of x-ray and visible wave mixing. Here the x-ray pulse (with a central angular frequency ω_x) is mixed with two nearly monochromatic optical pulses with central angular frequencies Ω_1 and Ω_2. Their frequency difference $\Delta\Omega$ corresponds to the shift required for the spectral interference pattern. In the x-ray and optical wave-mixing process, the dominant contribution to the nonlinear current density is originated from the inelastic scattering of the x-ray field by the optically induced charge distribution [18],

$$\begin{aligned} \vec{J}^{(2)}_{\omega_x+\Omega_{1/2}}(\vec{r},t) = \hat{\rho}^{(1)}_{\vec{G},\Omega_{1/2}}\vec{v}^{(1)}_{\omega_x} = \frac{iq}{4m\omega_x}\rho^{(1)}_{\vec{G},\Omega_{1/2}}E_x(\vec{r},t) \\ \times e^{i(\vec{k}_x+\vec{k}_{L,1/2}+\vec{G})\cdot\vec{r}-i(\omega_x+\Omega_{1/2})t}\hat{e}_x + \text{c.c.}, \end{aligned} \tag{2}$$

where $\vec{v}^{(1)}_{\omega_x}(\vec{r},t) = \frac{iqE_x(\vec{r},t)}{2m\omega_x}e^{i\vec{k}_x\cdot\vec{r}-i\omega_x t}\hat{e}_x + \text{c.c.}$ is the first-order induced velocity by the x-ray field, the x-ray pump pulse and the optically induced charge distribution are written as an envelope times a carrier wave $\hat{E}_x(\vec{r},t) = \frac{1}{2}E_x(\vec{r},t)e^{i\vec{k}_x\cdot\vec{r}-i\omega_x t}\hat{e}_x + \text{c.c.}$, $\hat{\rho}^{(1)}_{\vec{G},\Omega_{1/2}}(\vec{r},t) = \frac{1}{2}\rho^{(1)}_{\vec{G},\Omega_{1/2}}(\vec{r},t)e^{i(\vec{k}_{L,1/2}+\vec{G})\cdot\vec{r}-i\Omega_{1/2}t} + \text{c.c.}$, $\vec{k}_x$ and $\vec{k}_{L,1/2}$ are the wave vectors of the x-ray and the optical carrier fields, respectively, $\vec{G}$ is a specific reciprocal lattice vector, $\rho^{(1)}_{\vec{G},\Omega_{1/2}}$ is the $\vec{k}_{L,1/2}+\vec{G}$ spatial Fourier component of the optically induced charge distribution, m and q are the electron's mass and charge, respectively, and $\hat{e}_x$ is the x-ray pump polarization vector. We estimate the optically induced charge $\rho^{(1)}_{\vec{G},\Omega_{1/2}}$, which scales linearly with the IR or visible electric field, by using the tabulated indices of refraction at Ω_1 and Ω_2.

We consider here a scheme in which the two frequency-shifted replicas are generated in the same nonlinear medium (although more than one crystal may be used). This scheme minimizes the number of optical components, such as beam splitters and mirrors, required for the inspection of the pulse structure. A sketch of a possible setup for x-ray pulse characterization by spectral shearing interferometry using one nonlinear medium is shown in Fig. 1(a). Since the frequency shifts of the two generated replicas are different, they propagate in different directions, imposed by the phase-matching conditions as described in Fig. 1(b). However, since the k vector of the optical wave is much smaller than the k vectors of the x-ray waves and since dispersion in the x-ray regime is relatively weak, there are two possible approaches in which the spectral interference pattern could be obtained without additional x-ray optical components. The first approach is to impose that the two frequency-shifted replicas propagate in the same direction by simultaneous optimization of the phase mismatch for both frequency mixing processes. Both sum-frequency-generation (SFG) signals would propagate efficiently in the same direction as long as the crystal length is smaller than the coherence lengths of both processes. The second approach, which we choose for the following analysis, is to use the smallest possible angle between the two SFG beams while keeping the exact phase-matching conditions for both mixing processes. When using the second approach a spatial fringe pattern is added to the interference pattern described in Eq. (1). Fortunately, it is easy to generalize Eq. (1) to include this spatial fringe pattern, which is a simple oscillatory function in the case of no transverse phase variations. In the case where the measured pulse is not a plane wave, the retrieval of the spectral phase requires the knowledge of the spatial structure of the pulse. Note that the extraction of the phase difference $\varphi(\omega-\Omega_1) - \varphi(\omega-\Omega_2)$ is possible only when the phase between the two SFG beams is locked to a known value [20]. In addition, the third term of Eq. (1) should not be an even function of $\varphi(\omega-\Omega_1) - \varphi(\omega-\Omega_2)$, otherwise the sign of the requested phase difference cannot be resolved.

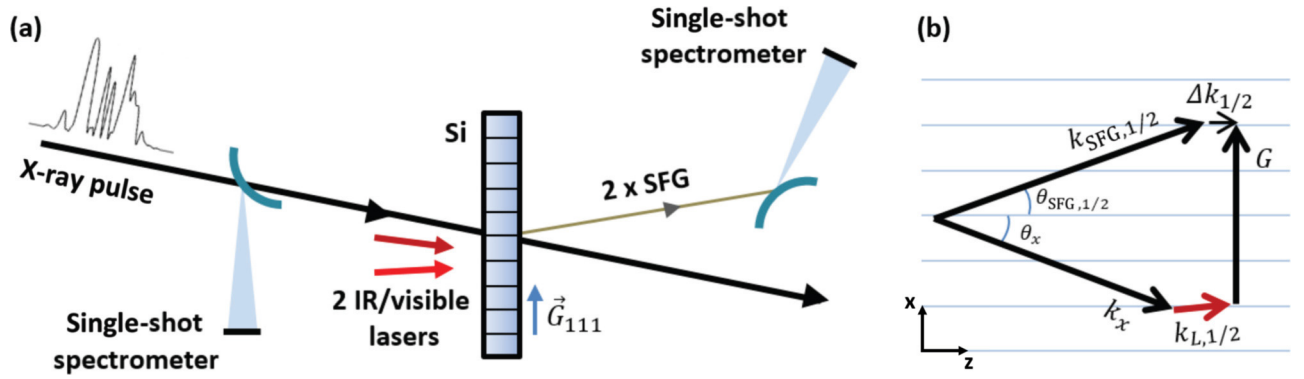

FIG. 1. (Color online) (a) Schematic example of the spectral shearing interferometer. A small fraction of the tested x-ray pulse is used for the measurement of its power spectrum. The pulse is mixed with two lasers with different optical frequencies in a nonlinear crystal. The generated signal is spectrally resolved to give the spectral shearing interference pattern from which the phase difference between neighboring spectral components is deduced. (b) Phase-matching diagram for the two SFG processes. The mismatch vector for each process is defined as $\Delta\vec{k}_{1/2} = \vec{k}_x + \vec{k}_{L,1/2} + \vec{G} - \vec{k}_{\mathrm{SFG},1/2}$.

Therefore, we choose to take $\phi_1 - \phi_2 = \frac{\pi}{2}$ for the following analysis.

We calculate the envelopes of the electric fields of sum-frequency-generated signals. We write the fields as $\hat{E}_{\mathrm{SFG},1/2}(\vec{r},t) = \frac{1}{2}E_{\mathrm{SFG},1/2}(\vec{r},t)e^{i\vec{k}_{\mathrm{SFG},1/2}\cdot\vec{r}-i(\omega_x+\Omega_{1/2})t}\hat{e}_{\mathrm{SFG},1/2} +$ c.c. The phase-matching conditions are $\Delta\vec{k}_{1/2} = \vec{k}_x + \vec{k}_{L,1/2} + \vec{G} - \vec{k}_{\mathrm{SFG},1/2} = 0$. The slowly varying envelope equation for each of the SFG fields with the nonlinear current densities described in Eq. (2) is as follows:

$$\sin(\theta_{\mathrm{SFG},1/2})\frac{\partial E_{\mathrm{SFG},1/2}}{\partial x} + \cos(\theta_{\mathrm{SFG},1/2})\frac{\partial E_{\mathrm{SFG},1/2}}{\partial z} + \frac{1}{v_{g,1/2}}\frac{\partial E_{\mathrm{SFG},1/2}}{\partial t} = -\frac{i\eta_{1/2}q}{4m\omega_x}(\hat{e}_x\cdot\hat{e}_{\mathrm{SFG},1/2})\rho^{(1)}_{\vec{G},\Omega_{1/2}}E_x(\vec{r},t), \tag{3}$$

where $v_{g,1/2}$ and $\eta_{1/2}$ are the group velocity and the wave impedance inside the crystal at the frequency $\omega_x + \Omega_{1/2}$, respectively. x and z are the coordinates in the scattering plane parallel and normal to the crystal surface, respectively. We choose the k-vectors of the pertinent beams to satisfy the exact phase-matching conditions for both mixing processes, where the two SFG fields are generated in the very nearly same direction.

In order to model temporally stochastic x-ray pulses, we assume an average Gaussian pulse envelope with pulse duration τ and bandwidth ΔE and construct a closely packed train of coherent Gaussian spikes with random phases as the following:

$$E(z',t) = \exp\left[-\frac{1}{\tau^2}\left(t-\frac{z'}{v_g}\right)^2\right]\sum_{n=-\infty}^{\infty}\exp[i\xi_n] \times\exp\left[-\frac{1}{\tau_0^2}\left(t-n\,\Delta\tau-\frac{z'}{v_g}\right)^2\right]. \tag{4}$$

Here z' is the propagation direction of the test pulse, $\tau_0 = \frac{2\sqrt{2\ln 2}\hbar}{\Delta E}$ is the duration of a transform-limited Gaussian pulse with full-width at half-maximum bandwidth ΔE ($\hbar$ being the reduced Planck constant), and $\Delta\tau$ is the duration between the spikes (taken to be $\Delta\tau = \frac{\tau_0}{5}$). Practically, the summation index n takes enough values so that the constituting spikes cover the Gaussian envelope. For each pulse we generate a set $\{\xi_n\}$ of uniformly distributed $[0,2\pi]$ random numbers. Similar to Ref. [21], the average over a large number of these stochastic pulses corresponds to the assumed average pulse structure. For simplicity, we consider a symmetric Gaussian (TEM_{00}) shape for the transverse field profile [22].

We solve Eq. (3) numerically by the fast-Fourier-transform method with respect to variables x and t and an integration with respect to z. The nonlinear medium we consider is a perfect silicon crystal. We assume that the (111) reflection is used to achieve phase matching and that the thickness of the crystal is 10 μm. We consider stochastic test pulses with an average bandwidth of 1 eV centered at 10 keV and polarized normal to the scattering plane. The average duration of the pulses is 20 fs, and the beam waist is 100 μm. The x-ray pulses are mixed with two IR quasimonochromatic plane-wave beams at 1.88 and 1.91 μm, both polarized in the scattering plane. The corresponding spectral distance between the optical pulses is $\Delta\Omega = 0.01$eV. The directions of propagation of the two lasers affect the efficiencies of the nonlinear processes (optimal with the polarization parallel to $\vec{G}$); the angle between the two SFG signals (which should be small in order to reduce the spatial interference) and their deviation from the Bragg angle (which should be large in order to reduce the elastic scattering of the test pulse). With the preference being a higher SFG efficiency and deviation from the Bragg angle than a smaller angle between the two SFG signals, we choose to take both laser beams almost perpendicular to $\vec{G}$ as in Fig. 1. With exact phase matching for both nonlinear processes giving an angle of 2.8° between both optical lasers, the angle between the propagation directions of the two SFG fields $\theta_{\mathrm{SFG},2} - \theta_{\mathrm{SFG},1}$ is 11.6 μrad, whereas their angular deviation from the Bragg angle is 413 μrad. We assume 1-ps optical pulses with a peak intensity of 10^{11} W/cm^2, which is below the IR damage threshold of silicon [24]. We note that with a pulse duration of 1 ps and a crystal length of 10 μm the group-velocity mismatch (GVM) between the x-ray and the optical pulses is negligible. However, there is a GVM between the x-ray test pulse and the SFG field, which limits the phase-matching bandwidth of

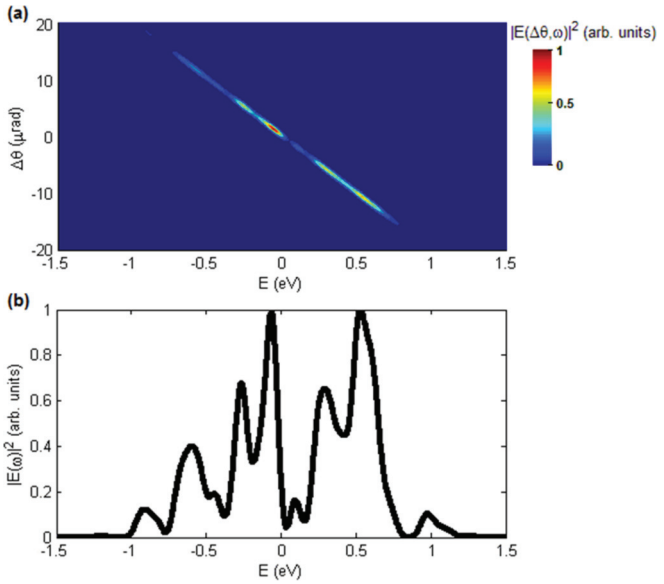

FIG. 2. (Color online) An example of the power spectrum for a signal generated by the two SFG processes. (a) The angular-spectral power distribution of the generated signal, showing the directions in which different portions of the spectrum propagate. (b) The power spectrum of the combined signal from the two generated SFG signals. This power spectrum portrays the concerning spectral interference pattern.

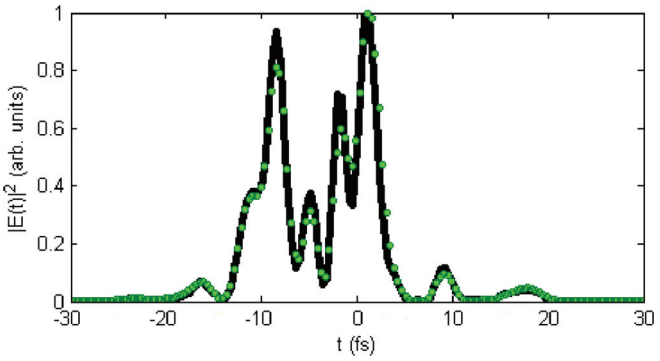

FIG. 3. (Color online) Reconstruction of a random x-ray pulse. The black solid line describes the temporal structure of a stochastic x-ray test pulse produced by the model described in Eq. (4). The green dots describe the reconstruction from the spectral interference pattern [Fig. 2(b)], obtained for the test pulse by using two nonlinear mixing processes with optical lasers at 1.88 and 1.91 μm as the shearing mechanism, the nonlinear medium being a 10-μm Si crystal and by using the power spectrum of the tested pulse.

the nonlinear process. We plot the power spectrum of the SFG signal in Fig. 2. For these parameters, the average efficiency of the x-ray and optical mixing is about 10^{-6}.

The full spectral interference pattern is distributed over an angular spread of about 30 μrad since different angles satisfy phase-matching conditions for different portions of the spectrum. This distribution constrains the angular tolerance of the single-shot spectrometer.

We use the power spectrum of the original test pulse, obtained by an additional single-shot spectrometer as shown in Fig. 1(a) and extract the phase differences $\varphi(\omega-\Omega_1)-\varphi(\omega-\Omega_2)$ from which the pulse spectrum (amplitude and phase) at sequential points $\tilde{E}(\omega_n)$ is calculated. Following that, an inverse Fourier transform of this spectrum is used to reconstruct the original temporal structure of the test pulse $E(t)$. An example of the reconstructed (green dots) and the original (black solid line) temporal structures is shown in Fig. 3.

We now discuss the practical limitations and constraints of the proposed scheme. One of the major challenges is that the amplitudes and the phases of the pulses emerging from the XFELs fluctuate randomly. Thus, the temporal structure of different pulses is substantially different. Consequently, the measurement of the spectral interference pattern requires the use of a single-shot spectrometer with a resolution that is adequate to capture significant phase variations over the pulse spectrum. Fortunately, several successful schemes for the shot-by-shot measurement of spiky XFEL pulses with spectral resolutions of 14 meV have been demonstrated [25–27].

A pulse-shape reconstruction is reliable only when the spectral interference of neighboring spectral components is revealed. The upper bound of the spectral difference $\Delta\Omega$ is limited by the Nyquist-Shannon sampling theorem. The lower bound of $\Delta\Omega$ is determined by the visibility of the interference and the ability of the apparatus to resolve the interference pattern. Furthermore, since only the phase differences between spectral components with difference $\Delta\Omega$ are measured, the characterization is incomplete if the spectral amplitude $A(\omega)$ is zero over a frequency interval larger than the spectral difference $\Delta\Omega$. In these cases, an additional similar scheme having a spectral shear greater than this interval is required in order to achieve the full characterization of the spectral phase.

The efficiency of the SFG process increases with the crystal length. However, there are several restrictions on the practical crystal thickness that may be used for spectral shearing. Since the coherence length of the nonlinear process is inversely proportional to the phase mismatch, a thin crystal is necessary to achieve a phase-matching bandwidth comparable to the bandwidth of the inspected pulses. In addition, spatial variations in the test pulses and the noncollinear geometry of the nonlinear process in thick crystals induce a spatiotemporal coupling, which adds distortions to the generated SFG fields, which thus blurs the temporal structure encoded in the interference pattern. These restrictions have been verified by further numerical simulations, varying the crystal thickness and assuming other diffraction planes, thus having different propagation geometries.

We note that a broad variety of spectral interferometry techniques have been developed [10]. The interferometric measurement can be performed, for example, by adding two beam splitters to the apparatus in Fig. 1(a), combining two sheared replicas of the test pulse into an interference pattern. In addition, it is possible to overcome the restriction of the narrow phase-matching bandwidth by using multiple apparatuses where each apparatus measures a different portion of the concerned pulse spectrum.

To summarize, we have described a method to fully characterize ultrashort hard x-ray pulses. The method is based on the spectral interference between two sheared replicas of

the original pulse, generated by three-wave mixing with IR or visible lasers. Practically, the scheme is limited by the efficiency and bandwidth of the x-ray and optical mixing process and by the performances of the single-shot spectrometer.

The proposed scheme has several important advantages: (1) It works on a single-shot basis and does not require moving parts. (2) The temporal jitter of the x-ray pulses does not influence the measurement since the duration of the optical pulse can be much longer than the maximum jitter. (3) The nonlinear medium can be a thin crystal to minimize propagation distortions. (4) The measured quantities are only the power spectra of the tested pulse and its interfering replicas. (5) The retrieval algorithm of the pulse structure is straightforward, and the only ambiguity is the global phase. We believe that the proposed scheme can be used to advance ultrafast x-ray science. For example, it may be used to improve the performances of XFELs in a manner similar to the characterization of ultrafast lasers in the optical regime and to enable the studies of new ultrafast effects.

This work was supported by the Israel Science Foundation (under Grant No. 1038/13).

[1] P. Emma *et al.*, Nat. Photonics **4**, 641 (2010).
[2] H. Tanaka *et al.*, Nat. Photonics **6**, 540 (2012).
[3] R. Neutze, R. Wouts, D. van der Spoel, E. Weckert, and J. Hajdu, Nature (London) **406**, 752 (2000).
[4] K. J. Gaffney and H. N. Chapman, Science **316**, 1444 (2007).
[5] M. Trigo *et al.*, Nat. Phys. **9**, 790 (2013).
[6] J. Küpper *et al.*, Phys. Rev. Lett. **112**, 083002 (2014).
[7] L. Young *et al.*, Nature (London) **466**, 56 (2010).
[8] B. W. Adams *et al.*, J. Mod. Opt. **60**, 2 (2013).
[9] W.-T. Liao, A. Pálffy, and C. H. Keitel, Phys. Rev. C **87**, 054609 (2013).
[10] I. A. Walmsley and C. Dorrer, Adv. Opt. Photonics **1**, 308 (2009).
[11] R. Trebino, *Frequency-Resolved Optical Grating: The Measurement of Ultrashort Laser Pulses* (Kluwer Academic, Boston, 2002).
[12] S. Shwartz *et al.*, Phys. Rev. Lett. **112**, 163901 (2014).
[13] K. Tamasaku *et al.*, Nat. Photonics **8**, 313 (2014).
[14] Y. Ding, C. Behrens, P. Emma, J. Frisch, Z. Huang, H. Loos, P. Krejcik, and M-H. Wang, Phys. Rev. Spec. Top.- Accel. Beams **14**, 120701 (2011).
[15] Y. Ding *et al.*, Phys. Rev. Lett. **109**, 254802 (2012).
[16] I. Grguraš *et al.*, Nat. Photonics **6**, 852 (2012).
[17] F. Quéré, J. Itatani, G. L. Yudin, and P. B. Corkum, Phys. Rev. Lett. **90**, 073902 (2003).
[18] T. E. Glover *et al.*, Nature (London) **488**, 603 (2012).
[19] C. Iaconis and I. A. Walmsley, Opt. Lett. **23**, 792 (1998).
[20] H. Miao, D. E. Leaird, C. Langrock, M. M. Fejer, and A. M. Weiner, Opt. Express **17**, 3381 (2009).
[21] S. D. Shastri, P. Zambianchi, and D. M. Mills, J. Synchrotron Radiat. **8**, 1131 (2001).
[22] We note that spatiotemporal variations in SPIDER at the optical regime have been developed by introducing a tilt between the two sheared replicas and using a two-dimensional single-shot spectrometer to resolve the spatiotemporal phase distribution [23].
[23] C. Dorrer, E. M. Kosik, and I. A. Walmsley, Opt. Lett. **27**, 548 (2002).
[24] B. M. Cowan, Proc. SPIE **6720**, 67201M (2007).
[25] D. Zhu, M. Cammarata, J. M. Feldkamp, D. M. Fritz, J. B. Hastings, S. Lee, H. T. Lemke, A. Robert, J. L. Turner, and Y. Feng, Appl. Phys. Lett. **101**, 034103 (2012).
[26] Y. Inubushi *et al.*, Phys. Rev. Lett. **109**, 144801 (2012).
[27] P. Karvinen *et al.*, Opt. Lett. **37**, 5073 (2012).